Metal Binding in Photosystem II Super- and Subcomplexes from Barley Thylakoids[1]

Sidsel Birkelund Schmidt, Daniel Pergament Persson, Marta Powikrowska, Jens Frydenvang, Jan K. Schjoerring, Poul Erik Jensen, and Søren Husted*

Plant and Soil Science (S.B.S., D.P.P., J.F., J.K.S., S.H.) and Molecular Plant Biology (M.P., P.E.J.) Sections, Copenhagen Plant Science Centre, Department of Plant and Environmental Sciences, Faculty of Science, University of Copenhagen, DK–1871 Frederiksberg C, Denmark

ORCID IDs: 0000-0002-4193-4454 (S.B.S.); 0000-0001-9294-1227 (J.F.); 0000-0002-2852-3298 (J.K.S.); 0000-0001-6524-7723 (P.E.J.); 0000-0003-2020-1902 (S.H.).

Metals exert important functions in the chloroplast of plants, where they act as cofactors and catalysts in the photosynthetic electron transport chain. In particular, manganese (Mn) has a key function because of its indispensable role in the water-splitting reaction of photosystem II (PSII). More and better knowledge is required on how the various complexes of PSII are affected in response to, for example, nutritional disorders and other environmental stress conditions. We here present, to our knowledge, a new method that allows the analysis of metal binding in intact photosynthetic complexes of barley (*Hordeum vulgare*) thylakoids. The method is based on size exclusion chromatography coupled to inductively coupled plasma triple-quadrupole mass spectrometry. Proper fractionation of PSII super- and subcomplexes was achieved by critical selection of elution buffers, detergents for protein solubilization, and stabilizers to maintain complex integrity. The applicability of the method was shown by quantification of Mn binding in PSII from thylakoids of two barley genotypes with contrasting Mn efficiency exposed to increasing levels of Mn deficiency. The amount of PSII supercomplexes was drastically reduced in response to Mn deficiency. The Mn efficient genotype bound significantly more Mn per unit of PSII under control and mild Mn deficiency conditions than the inefficient genotype, despite having lower or similar total leaf Mn concentrations. It is concluded that the new method facilitates studies of the internal use of Mn and other biometals in various PSII complexes as well as their relative dynamics according to changes in environmental conditions.

Several metals are important for chloroplast functioning, particularly in the photosynthetic apparatus, where they act as cofactors and catalysts in electron transport processes (Merchant, 2006; Nouet et al., 2011; Yruela, 2013). The photosynthetic biometals include iron (Fe) in the form of Fe-S clusters in PSI, heme-bridged Fe (cytochrome b_{559}) and nonheme Fe in PSII, copper (Cu) in plastocyanin, magnesium (Mg) in chlorophyll (Chl), and calcium (Ca) and manganese (Mn) in PSII. Mn has a very special role because a metal cluster of four Mn ions and one Ca ion comprises the catalytic center of the oxygen evolving complex (OEC) in PSII (Ono et al., 1992; Umena et al., 2011). In the OEC, water is split, and molecular oxygen is produced by the photosynthetic light reactions. The photosynthetic biometals are, however, highly reactive and involved in a multitude of side reactions, which constitute a challenge for metal homeostasis. Accordingly, the handling of metals must be tightly regulated, and they must be kept within specific concentration ranges inside living cells to ensure adequate supply, while at the same time, avoiding oxidative stress (Pakrasi et al., 2001; Shcolnick and Keren, 2006; Møller et al., 2007).

PSII is a large pigment-protein complex localized in the grana regions of the thylakoid membrane of chloroplasts. The basic structure of PSII is a monomer, and each complex contains more than 40 different proteins bound either stably or transiently (Nelson and Yocum, 2006; Shi et al., 2012; Järvi et al., 2015). The luminal surfaces of PSII are associated with the extrinsic proteins PsbO, PsbP, and PsbQ, which shield and support the catalytic Mn cluster and are required for efficient oxygen evolution (Roose et al., 2007; Bricker et al., 2012; Liu et al., 2014). After dimerization of the monomer, the complex associates with multiple copies of the light-harvesting antenna complex II (LHCII), forming various types of functional PSII-LHCII supercomplexes (Tikkanen et al., 2008; Kouřil et al., 2012; Shi et al., 2012).

Intact PSII-LHCII supercomplexes have been successfully isolated, characterized, and refined from, for example, pea (*Pisum sativum*; Barera et al., 2012), Arabidopsis (*Arabidopsis thaliana*; Caffarri et al., 2009),

[1] This work was supported by Innovation Fund Denmark (NUTRIEFFICIENT; grant no. 10–093498) and the VILLUM Research Center for Plant Plasticity.

* Address correspondence to shu@plen.ku.dk.

The author responsible for distribution of materials integral to the findings presented in this article in accordance with the policy described in the Instructions for Authors (www.plantphysiol.org) is: Søren Husted (shu@plen.ku.dk).

S.H. and S.B.S. conceived the research plans; S.H. and P.E.J. supervised the experiments; S.B.S. performed all the experiments; D.P.P. and M.P. provided technical assistance to S.B.S.; S.H., P.E.J., and S.B.S. designed the experiments and analyzed the data; J.F. performed the peak fitting of chromatographic data; S.B.S. and S.H. conceived the project and wrote the article with contributions of all the authors; J.K.S. supervised and complemented the writing.

www.plantphysiol.org/cgi/doi/10.1104/pp.15.00559

and green algae (*Chlamydomonas reinhardtii*; Tokutsu et al., 2012). The procedure has typically involved Suc density gradient ultracentrifugation. Also, blue native (BN)-PAGE has been optimized for the separation and proteomic characterization of thylakoid PSII-LHCII supercomplexes (Heinemeyer et al., 2004; Järvi et al., 2011; Pagliano et al., 2014). The supramolecular organization of isolated PSII is very much dependent on the choice of detergent for efficient solubilization of the membrane-bound photosynthetic pigment-protein complexes. In recent years, dodecyl maltoside (DM) has become a commonly used detergent for one-step isolation of integral membrane proteins and complexes from thylakoids (Eshaghi et al., 1999; van Roon et al., 2000; Dekker et al., 2002; Pagliano et al., 2011). This detergent exists in two isomeric forms (α-DM and β-DM), of which α-DM is a milder detergent than β-DM, thereby better preserving the integrity of large PSII-LHCII supercomplexes (Pagliano et al., 2012).

The major challenge associated with purification of higher plant PSII-LHCII supercomplexes is to obtain and subsequently, maintain the integrity of PSII super- and subcomplexes, including cofactors and the extrinsic proteins. To prevent dissociation of biometals and the extrinsic proteins from PSII, the osmoprotectant betaine (Papageorgiou et al., 1991; Papageorgiou and Murata, 1995) has successfully been included in the buffer of Suc gradients (Boekema et al., 1998; Tokutsu et al., 2012). Although the above-mentioned methods primarily have focused on the characterization and structural organization of isolated PSII-LHCII supercomplexes, no bench-top method has been available that allows direct analysis of the actual metal binding in PSII super- and subcomplexes. Such a method is required in order to fully understand how Mn and other photosynthetic biometals interact with the photosynthetic complexes, in particular PSII, and how the metal binding affects PSII dynamics under changing environmental conditions, including plant nutritional disorders.

We here present a robust and highly sensitive method for analysis of metal binding in PSII-LHCII super- and subcomplexes from isolated barley (*Hordeum vulgare*) thylakoids. The method is based on size exclusion chromatography (SEC) coupled to inductively coupled plasma (ICP) triple-quadrupole (QQQ) mass spectrometry (MS). SEC is a gentle protein separation technique, provided that the stationary and mobile phases are carefully selected. Using an optimized set of analytical conditions, it is possible to maintain the integrity of metalloprotein complexes (Persson et al., 2009; Husted et al., 2011). We systematically evaluate the essential and important factors required to obtain optimal chromatographic resolution while maintaining PSII integrity, focusing on choice of mobile phase, detergents, stabilizers, and the most suitable chromatographic columns for efficient protein fractionation and elution. The optimized method, with its multielement ability, enables the study of metal binding in PSII-LHCII super- and subcomplexes. To show the applicability of the method, we studied the metal profiles of barley thylakoids that had been isolated from plants with different levels of Mn deficiency. Mn binding in size-fractionated PSII complexes was evaluated in response to increasing Mn deficiency, and two genotypes differing in their tolerance to Mn deficiency were compared.

RESULTS AND DISCUSSION

The first step in the method development focused on optimization of the conditions for solubilization and separation of PSII complexes from barley 'Antonia' and 'Vanessa' thylakoids. In the second step, we improved the integrity and stability of size-fractionated PSII complexes. The third step included biochemical characterization and identification of Mn- and Fe-containing fractions. The applicability of the method was shown by quantification of Mn binding to PSII in thylakoids of two barley genotypes with contrasting Mn efficiency exposed to increasing levels of Mn deficiency. The various steps in development and validation of the method are described in the following sections.

Optimization of Conditions for Solubilization and Fractionation of Thylakoid Membranes

Before ICP-QQQ-MS analysis, barley thylakoids were solubilized using either the α-DM or β-DM isomeric form of the detergent and loaded onto a size exclusion column.

Mobile Phase

Three mobile phases, ammonium acetate (AmAc), Tricine, and Bis-Tris, were tested for their ability to separate photosynthetic pigment-protein complexes with the highest possible Mn binding (i.e. indicative of PSII complexes). AmAc is a potentially volatile mobile phase and consequently ideally suited for ICP-MS systems. Tricine and Bis-Tris are two frequently used buffers in analyses of photosynthetic proteins, the latter being a commonly used solubilization buffer (Järvi et al., 2011). During the chromatographic separation, the mobile phase, the sampler, and the column were kept cold because the temperature previously has been shown to have a major effect on the stability of the complexes (Caffarri et al., 2009).

The composition of the mobile phase turned out to have a remarkable effect on the integrity of the metalloprotein complexes. Excellent fractionation of the Mn protein complexes was obtained using 25 mM Bis-Tris as the mobile phase (Fig. 1). When using Tricine as the elution buffer, the fractionation of Mn-containing complexes was inadequate compared with Bis-Tris, whereas AmAc as the mobile phase resulted in an acceptable fractionation compared with Tricine, but the integrity of the Mn protein complexes was reduced (Fig. 1).

Detergent

Four distinguishable fractions (peak shoulders), eluting at 468, 522, 545, and 573 s, were observed when α-DM was used as the detergent (R_1–R_4 in Fig. 1,

upper). In contrast, only three fractions, eluting at 530, 546, and 572 s, could be discerned using β-DM for solubilization (R_1–R_3 in Fig. 1, lower). The choice of the ideal detergent is pivotal to recover the large and fragile PSII supercomplexes for additional analysis. This was evidenced by the earlier elution of the first two Mn-containing fractions (R_1 and R_2 in Fig. 1, upper versus lower), indicating that larger photosynthetic complexes were preserved from thylakoids subjected to α-DM solubilization compared with β-DM. This supports that α-DM was more gentle to the photosynthetic complexes than its β-isomeric form, and it underlines its superiority in terms of maintaining complex integrity (Pagliano et al., 2012), allowing studies of Mn binding in the largest PSII-LHCII supercomplexes. In accordance with α-DM being a milder detergent than its β-isomeric form it has previously been shown that α-DM-solubilized PSII supercomplexes bound more LHCII and retained stoichiometric amounts of the extrinsic subunits of PSII (PsbO, PsbP, and PsbQ), whereas most PsbP and PsbQ were lost when using β-DM for solubilization (Barera et al., 2012; Tokutsu et al., 2012).

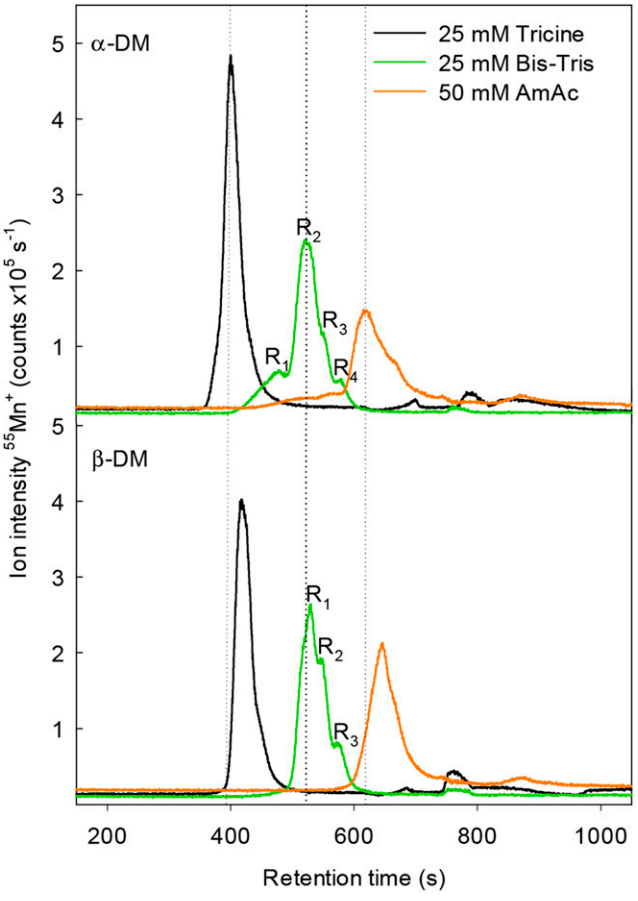

Figure 1. SEC-ICP-QQQ-MS chromatogram showing the Mn elution profiles of α-DM-solubilized thylakoids (upper) and β-DM-solubilized thylakoids (lower) using Tricine, Bis-Tris, or AmAc as the mobile phase. R_X indicates the number of peaks (or shoulders) that could be resolved using Bis-Tris as the mobile phase.

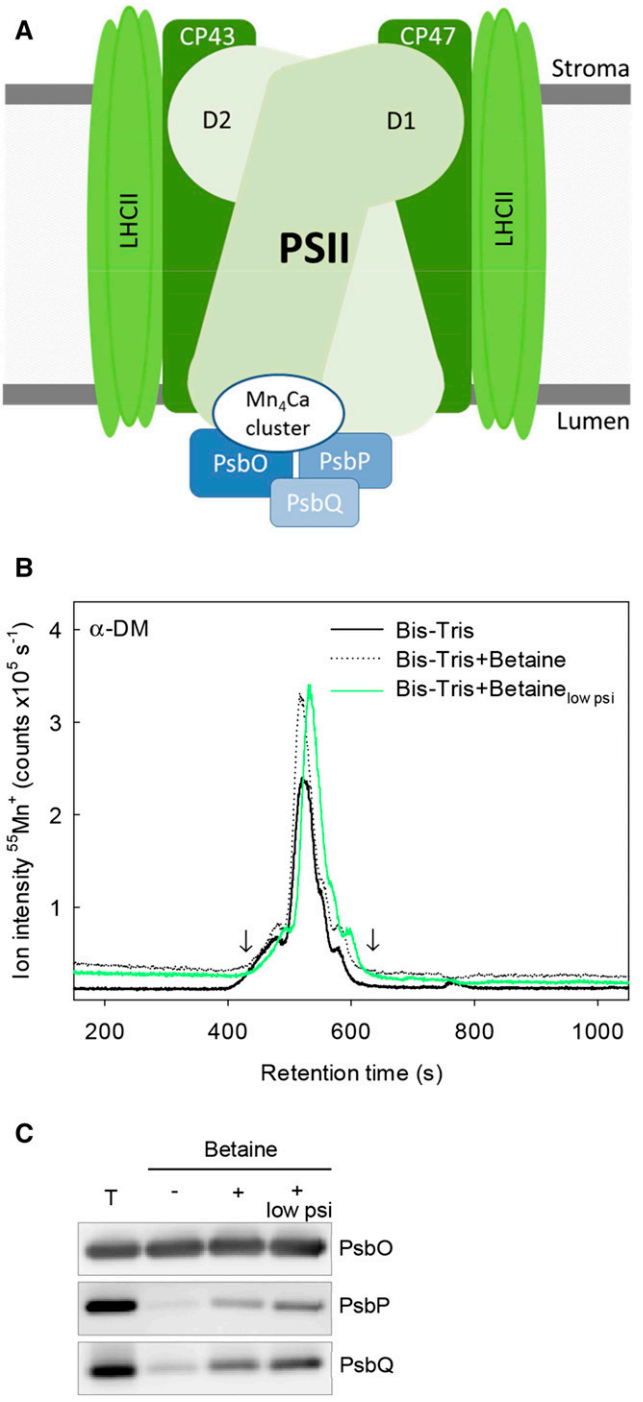

Figure 2. A, Simplified scheme showing the extrinsic proteins on the luminal side of PSII. In higher plants, the extrinsic proteins are PsbO (33 kD), PsbP (23 kD), and PsbQ (17 kD), and these proteins stabilize the Mn_4Ca cluster. B, SEC-ICP-QQQ-MS chromatogram where the ion intensity of Mn is monitored against the retention time. The chromatogram illustrates the fractionation of α-DM-solubilized thylakoid proteins using Bis-Tris as the mobile phase with or without betaine and reduced column pressure (low psi). Arrows indicate the heart-cut Mn fraction used in western-blot analysis (C) with antibodies against extrinsic subunits PsbO, PsbP, and PsbQ of thylakoids (lane T) and the heart-cut Mn fraction (eluting from 435 to 609 s; arrows in B) using Bis-Tris (lane 2) or Bis-Tris including betaine (lanes 3 and 4 [reduced column pressure]); 3 μg of protein was loaded on each lane.

Improving the Integrity and Stability of Size-Fractionated PSII Complexes

Stabilization by Addition of Betaine to the Mobile Phase

Ideal separation conditions should be able to maintain the integrity of PSII complexes. To further stabilize the fractionated PSII super- and subcomplexes, 0.5 M betaine was added to the mobile phase. The rationale for this approach was to preserve the attachment of the extrinsic proteins PsbO, PsbP, and PsbQ (Fig. 2A). These proteins have previously been found to be partly removed during purification of PSII (Boekema et al., 1995, 1998). Importantly, the betaine addition did not alter the quality of separation (resolution) or the retention time of the Mn binding protein complexes (Fig. 2B).

After collection of the entire Mn-containing fraction eluting between 420 and 618 s (arrows in Fig. 2B), the integrity of the isolated PSII super- and subcomplexes was explored with or without betaine added to the mobile phase. For this purpose, western-blot analysis with specific antibodies raised against the extrinsic proteins of PSII was used (Fig. 2C). Of the three OEC subunits in barley, PsbO was least sensitive to the chromatographic separation, which was shown by the fact that this subunit was present in nearly the same quantity in the collected Mn-containing fraction, regardless of betaine addition to the mobile phase (Fig. 2C, lanes 2 and 3). This clearly shows that PsbO is tightly bound to PSII, which is in line with the observations by Caffarri et al. (2009). The pronounced stability of PsbO can most likely be attributed to its interaction with several PSII core subunits that stabilize the binding (Umena et al., 2011). The extrinsic proteins together with PSII core proteins were also found to be present in the Mn-containing fractions when analyzed by shotgun proteomics (Supplemental Table S1).

In contrast to PsbO, the amounts of PsbP and PsbQ retained in the PSII complexes were almost absent without betaine in the mobile phase, showing a marked dissociation of these proteins, either during solubilization, during the chromatographic separation, and/or during the subsequent concentration on spin filters of the collected fraction (Fig. 2C, lane 2). A major analytical challenge is that the interaction of PsbP and PsbQ with the PSII core is readily disrupted already during the solubilization procedure (Ifuku et al., 2011). Addition of betaine to the mobile phase greatly increased the proportion of attached PsbP and PsbQ (Fig. 2C, lane 3). Hence, the addition of betaine was crucial for preserving the integrity of PSII super- and subcomplexes.

Additional Stabilization by Lowering the Column Pressure

The OEC subunits, especially PsbP, were retained to an even greater extent when the column pressure was lowered from 2,100 pounds per square inch (psi) to approximately 1,300 psi by changing the diameter of the tubing connecting the column with the HPLC system (Fig. 2C, lane 4). This finding reflects the impact of mechanical stress causing slight dissociation of the extrinsic proteins from PSII. Importantly, no significant change in the ion intensity of Mn in the fractionated PSII complexes could be observed (Fig. 2B). Because of the easier operation and simultaneous UV-Vis detection, normal pressure separation (2,100 psi) was chosen as the optimal approach.

Verification of Integrity of PSII Super- and Subcomplexes

As additional evidence for PSII integrity, the photosynthetic activity in heart-cut Mn-containing fractions was measured. This showed that the collected Mn fraction evolved oxygen in rates between 15 and 35 μmol O_2 mg $(Chl)^{-1}$ h^{-1}. The PSII complexes were thus biologically active under the experimental conditions used. However, the oxygen evolution rates were lower compared with the rates obtained on intact thylakoids, indicating losses in PSII functionality caused by the solubilization process and/or the following chromatographic separation conditions. This might reflect a partial retention of the extrinsic proteins PsbP and PsbQ because all three extrinsic proteins have been shown to influence oxygen evolution (Bricker et al., 2012; Järvi et al., 2013). The oxygen evolution measurements were, furthermore, complicated by the small sample amounts loaded on the column, resulting in the requirement of numerous collections in order to obtain enough sample material for oxygen evolution measurements. To further verify the integrity of PSII super- and subcomplexes, the signal intensities of Mn and Ca from four independent thylakoid preparations were recorded simultaneously (Supplemental Fig. S1) and subsequently converted into a molar Mn to Ca ratio (Supplemental Fig. S2). From the ratio signal (Supplemental Fig. S2), a molar ratio between 4 and 5 is observed at a retention time around 500 s, where the overlapping signals from the additional Mn and Ca peaks are minimal. To obtain an accurate estimate of the molar Mn to Ca ratio, peak fitting was performed using sums of Exponentially Modified Gaussian (EMG) profiles (Supplemental Fig. S3; Di Marco and Bombi, 2001). Assuming that the largest Mn peak and the first Ca peak, with a molecular mass about 900 kD, represent active PSII supercomplexes, the area of the corresponding fitted peaks resulted in a molar Mn to Ca ratio of 4.1 $\pm$ 0.6 (n = 4). This estimate is very encouraging considering the theoretical ratio of 4 in the Mn cluster of PSII (Umena et al., 2011), thereby strengthening the observations that the fractionated PSII complexes are catalytically competent and that the measurements are essentially free from interferences caused by unspecifically bound Mn and other Mn metalloproteins.

Final Selection of Optimal Conditions for Separation of PSII Super- and Subcomplexes

The comprehensive method optimization clearly showed that PSII as a metalloprotein complex is extremely sensitive to the physical and chemical environment used for extraction and separation. Based on the above results, the selection of α-DM as the detergent combined with

Bis-Tris as the mobile phase were able to provide superior chromatographic resolution. In addition, betaine may be included in the mobile phase as a stabilizer to retain the integrity of the fractionated PSII complexes, including the extrinsic proteins. This set of conditions allowed online SEC-ICP-QQQ-MS measurements of metal binding in size-fractionated, highly intact, and catalytically competent photosynthetic complexes of barley thylakoids.

Identification of Fractionated Photosynthetic Complexes

Characterization of Mn- and Fe-Containing Complexes

Using the optimized separation conditions, a multielement analysis with corresponding UV-Vis elution profiles was performed to further explore the eluting photosynthetic Mn- and Fe-containing pigment-protein complexes of barley thylakoids (Fig. 3, A and B). Indeed, the Mg elution profile and the UV-Vis signals measured at 280 nm (protein) and 663 nm (Chl) were completely overlapping, clearly showing that the pigment-protein complexes are reflected by the UV-Vis and Mg signals (Fig. 3B). During the analysis, the ion intensities of Mg (proxy for Chl), Fe (proxy for PSI), S (proxy for Cys- or Met-containing proteins), and Mn (proxy for PSII) were analyzed simultaneously in a single chromatographic run (Fig. 3A). The first eluting Mn-containing fraction (R_1 in Fig. 1, upper) was omitted because of the relatively low Mn intensity and the fact that it most likely contained membrane fragments that were not sufficiently solubilized (Pagliano et al., 2012).

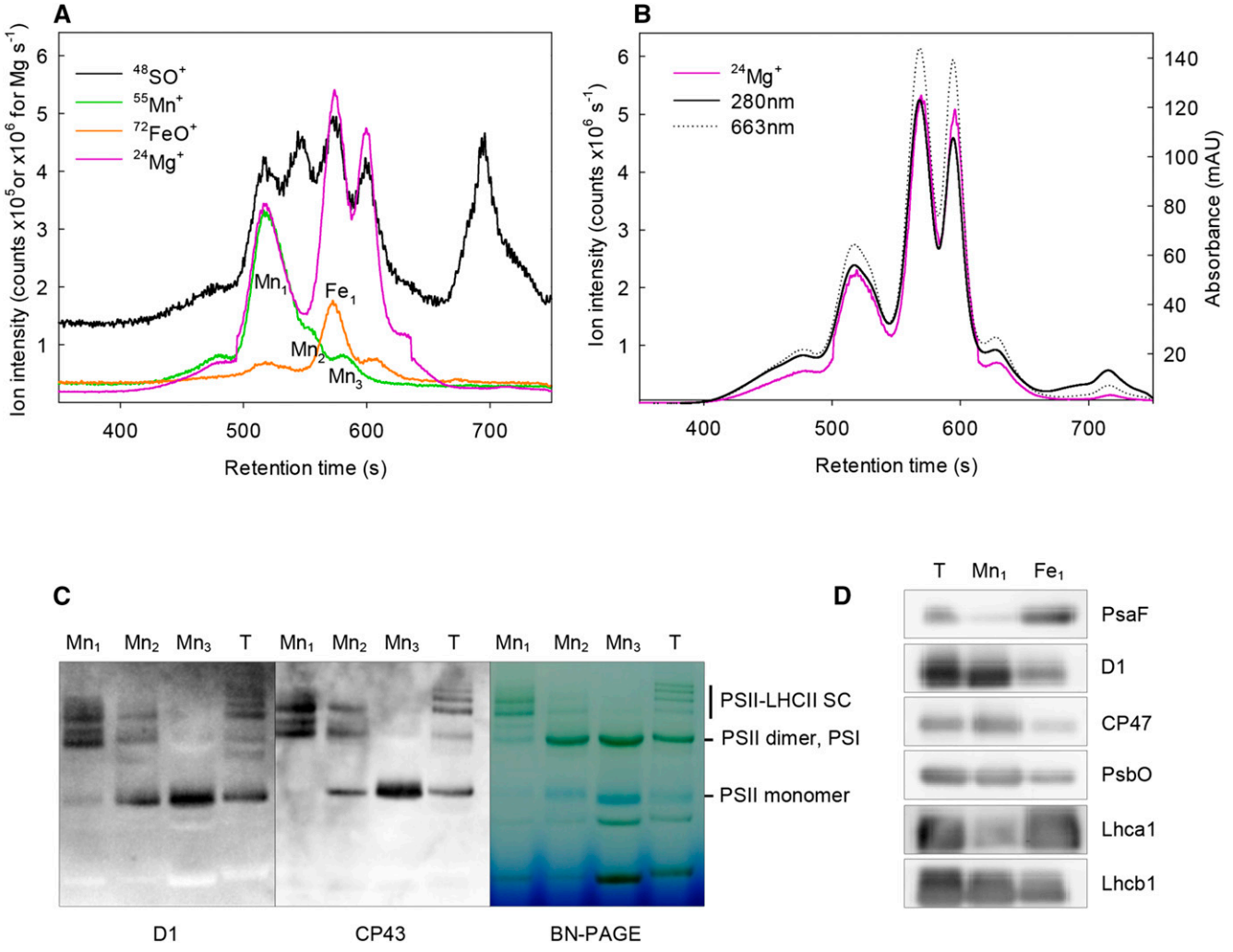

Figure 3. A, Optimized multielement chromatogram. Size exclusion profiles recorded for the nonoxide ions $^{24}Mg^+$ and $^{55}Mn^+$ and the oxide ions of $^{48}SO^+$ and $^{72}FeO^+$. Individual PSII subfractions (Mn_1, Mn_2, and Mn_3) and the PSI fraction (Fe_1) were collected. B, UV-Vis elution profiles measured at 280 and 663 nm together with the $^{24}Mg^+$ ion intensity signal (mAU, Milli absorption units). C, BN-PAGE gel of PSII subfractions (Mn_1, Mn_2, and Mn_3) followed by western blotting using antibodies against the D1 and CP43 subunits. Lane T represents barley thylakoids and was included as a size marker. An equal volume was loaded on each lane. SC, Supercomplex. D, Western-blot analysis with antibodies against PsaF, D1 and CP47 core proteins of PSII, extrinsic subunit PsbO, and antenna proteins Lhca1 and Lhcb1 of Mn_1 and Fe_1 subfractions and barley thylakoids (lane T); 2.5 μg of total protein was loaded on each lane.

Table I. *Spectroscopic details of the major Mn- and Fe-containing fractions*

Spectroscopic details of fractions Mn_1 and Fe_1 characterized by their retention times (rTs) from the size exclusion chromatogram (Fig. 3A). From the spectra of each peak (Supplemental Fig. S4), the A_{480} to A_{410} and the A_{700} to A_{670} ratios were calculated, and the wavelength of the maximum absorption (λ_{max}) in the red absorption region of the Chl was determined. Values are based on a single but typical chromatogram of α-DM-solubilized thylakoids using Bis-Tris as the mobile phase.

Fraction	rT	A_{480} to A_{410}	A_{700} to A_{670}	λ_{max}
	s			*nm*
Mn_1	517	0.70	0.09	677.0
Fe_1	572	0.54	0.24	679.4

The identities of the major Mn- and Fe-containing fractions were assigned based on element composition (Fig. 3A) and the band intensity of collected Mn fractions were analyzed by BN-PAGE followed by western blotting (Mn_1–Mn_3 in Fig. 3C). The Mn_1 and Fe_1 fractions were further subjected to conventional immunoblot analysis of protein composition (Fig. 3D), and their spectroscopic characteristics were considered (Table I; Supplemental Fig. S4). With respect to the latter, the A_{480} to A_{410} ratio roughly monitors the ratio between Chl *b* and Chl *a* (carotenoids also contribute to absorption at 480 nm to some extent), whereas the A_{700} to A_{670} ratio provides information about the relative content of long wavelength-absorbing Chls predominantly present in PSI (van Roon et al., 2000; Dekker et al., 2002; Pagliano et al., 2012).

Metal Profiles of Thylakoids Are Correlated to Fractionated PSII and PSI Complexes

To confirm that the metal content probed by the ICP-QQQ-MS is correlated to the fractionated photosynthetic complexes, we used a barley mutant, *viridis zb63*, that is essentially devoid of PSI. This mutant has a mutation causing PSI depletion, thereby representing an in vivo model of PSII (Marr et al., 1996; Nielsen et al., 1996; Scheller et al., 2001; Morosinotto et al., 2006). Solubilized thylakoids from the PSII active mutant were analyzed by ICP-QQQ-MS using α-DM and Bis-Tris as the mobile phase. The Mn (proxy for PSII) and Fe (proxy for PSI) profiles of the size-fractionated photosynthetic complexes were recorded (Supplemental Fig. S5). The Mn chromatogram (Supplemental Fig. S5A) showed an identical signal of size-fractionated Mn-containing protein complexes for the wild type and the *viridis zb63* mutant, whereas the corresponding Fe chromatogram (Supplemental Fig. S5B) indicated that the largest Fe peak represents PSI because this peak is absent in the signal from *viridis zb63*. It can, therefore, be concluded that Mn fractions and the largest Fe fraction are enriched in PSII complexes and PSI, respectively.

Mn-Containing Fractions

As verified by analyzing the PSI-less barley mutant *viridis zb63*, all Mn-containing fractions contain PSII. Below, the macromolecular structures of the various PSII fractions are characterized in further detail.

The major Mn-containing fraction (Mn_1 in Fig. 3A), having a molecular mass of about 900 kD, perfectly coeluted together with the chromatographic signals of Mg, Fe, and S. The multielement chromatogram together with the spectroscopic details (Table I) indicated that this fraction was enriched in PSII (the absorption spectrum peaked at 677 nm; extremely low A_{700} to A_{670} ratio value) and LHCII (high A_{480} to A_{410} ratio and a relatively high Mg content). The BN-PAGE results showed a marked enrichment in PSII-LHCII supercomplexes when comparing the composition of the Mn_1 fraction (Fig. 3C, lane 1) with the thylakoid marker (T in Fig. 3C). Finally, the western-blot analysis showed that the fraction was dominated by the PSII core proteins D1 and CP47, the antennae protein of Lhcb1, and the extrinsic subunit PsbO (Fig. 3D). We therefore conclude that this fraction contained PSII-LHCII supercomplexes. The fraction also contained small amounts of PSI as evidenced by the presence of PsaF and Lhca1 proteins in the western-blot analysis (Fig. 3D).

The second Mn-containing fraction (Mn_2 in Fig. 3A) presumably contained a large proportion of dimeric PSII. In BN-PAGE, PSII dimers and PSI coelute and cannot be distinguished (Fig. 3C). However, considering the molecular mass to be about 505 kD, the relatively high Mn content, and the low Fe content (Fig. 3A), it is most likely that dimeric PSII was dominating this fraction. This was further visualized by BN western blots with D1 and CP43 antibodies of the fraction (Fig. 3C); however, these blots also indicated that the fraction partly contained the smallest PSII supercomplexes together with PSII monomers.

Clearly, the third and last Mn-containing fraction eluting (Mn_3) was enriched in PSII monomers according to results from the BN-PAGE analysis and subsequent immunoblot analysis indicating the presence of D1 and CP43 (Mn_3 in Fig. 3C). Furthermore, according to the elution time, this PSII fraction was about one-half the molecular mass of the Mn_2 fraction (300 versus 505 kD).

Fe-Containing Fractions

The major Fe-containing fraction (Fe_1) with a molecular mass of 348 kD contained PSI complexes coeluting with dimeric and monomeric PSII. The high Fe content is in agreement with the fact that there are 12 Fe atoms per PSI protein complex compared to 3 Fe atoms per PSII complex (Raven et al., 1999). In addition, the Fe_1 peak coeluted with Mg, S (Fig. 3A), and Ca (Supplemental Fig. S6), indicating that this fraction represents a stable PSI pigment-protein complex with LHC attached. It can be speculated that PSI contains Ca, which was indicated by a rather high Ca signal in the PSI-enriched fraction (Supplemental Fig. S6). In cyanobacteria (*Thermosynechococcus elongatus*), Ca has been shown to be important for PSI trimerization

(Jordan et al., 2001; Grotjohann and Fromme, 2005), adding an interesting perspective for additional research on the putative role of Ca in higher plant PSI.

The spectroscopic characteristics of the Fe_1 fraction (Table I) show that Fe_1 is peaking at 679.4 nm together with a low A_{480} to A_{410} ratio (0.54) and a high A_{700} to A_{670} ratio (0.24), which is typical for PSI-containing fractions (Pagliano et al., 2012). BN-PAGE analysis of Mn_3, which is partly overlapping with Fe_1, shows a band that can be assigned to PSI because there is no signal for D1 or CP43 in this band (Mn_3 in Fig. 3C). By exploring the protein composition of Fe_1 (Fig. 3D), it was further evident that the abundance of PsaF and Lhca1 were enriched/more pronounced in this fraction compared with Mn_1.

As shown by the above results, the multielement chromatogram did not only provide information about PSII complexes, but could also be used to gain information about the relative PSI content. To rule out contamination with Mn-containing proteins not associated with the photosynthetic complexes, we performed proteomic analysis of the Mn_1 and Fe_1 heat-cut fractions. This confirmed that no known Mn-containing protein contaminants (Mn superoxide dismutase and oxalate oxidase) were present in the solubilized thylakoid samples (Supplemental Table S1).

Mn Binding in Various PSII Complexes as Affected by Mn Deficiency

The applicability of the SEC-ICP-QQQ-MS-based method was shown by analyzing thylakoids from barley plants grown at four different Mn levels corresponding to control and mild, moderate, and severe Mn deficiency. Two genotypes previously described to

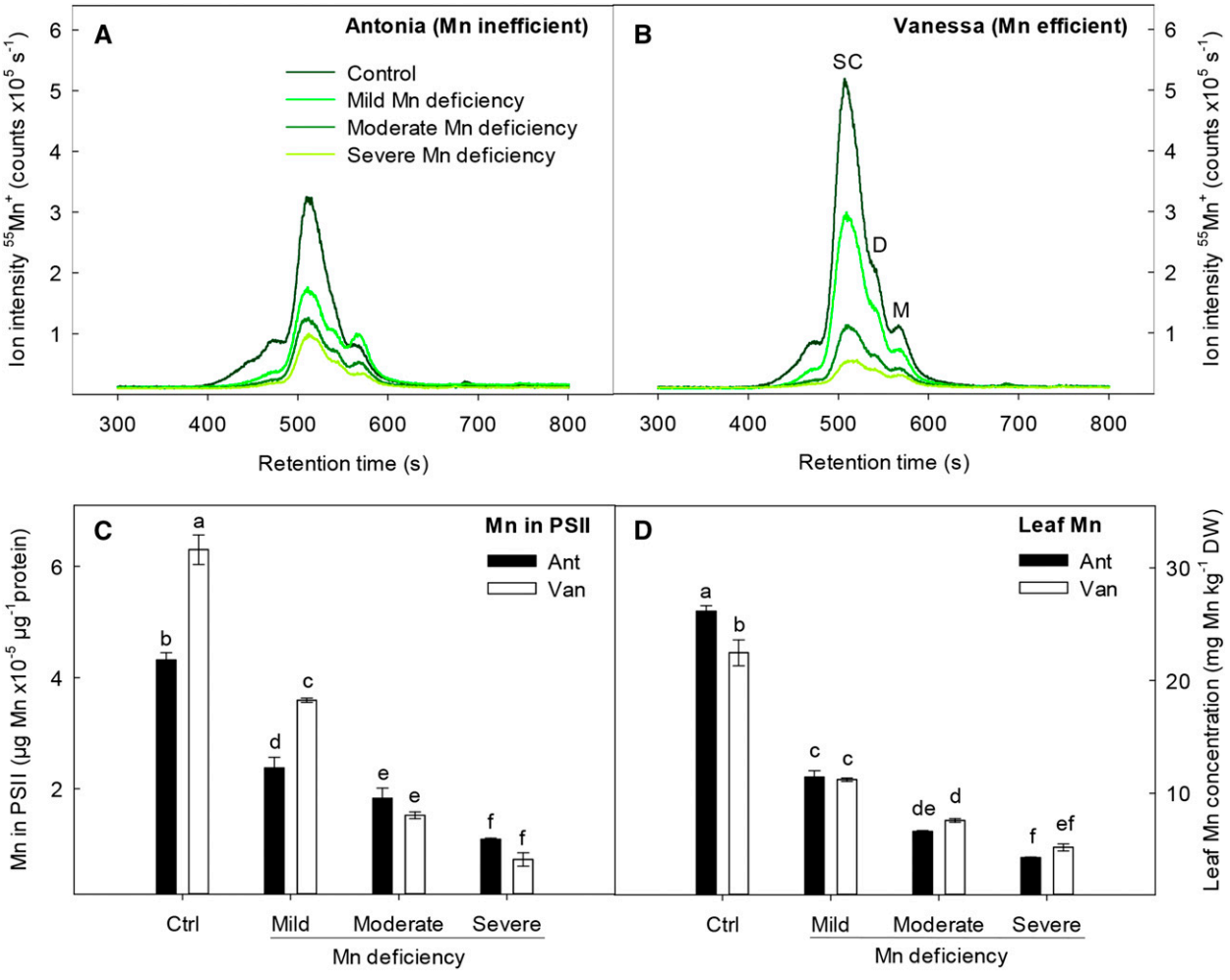

Figure 4. Representative Mn SEC-ICP-QQQ-MS chromatograms (raw data) of thylakoids isolated from control (Ctrl) plants or plants exposed to mild, moderate, or severe Mn deficiency for the Mn-inefficient genotype cv Antonia (A) and Mn-efficient genotype cv Vanessa (B). Fractionated PSII complexes were indexed as follows: PSII-LHCII supercomplex (SC), dimer (D), and monomer (M). Mn bound in PSII (C) and total leaf Mn concentration (youngest fully emerged leaves; D). Values are means ± SE (n = 3). Bars with the same letter are not significantly different ($P \geq 0.05$). DW, Dry weight.

widely differ in their sensitivity to Mn deficiency (Husted et al., 2009) were included in the experiment to further investigate the physiological mechanisms by which Mn-efficient barley genotypes cope with limited Mn availability. The new method presented here facilitates the study of how the various complexes of PSII respond to increasing severity of Mn deficiency, and in the following case studies it was used to (1) visualize the dynamics of PSII during the progression of Mn deficiency and (2) investigate differences in Mn binding in PSII between the two genotypes under control and Mn-limiting conditions.

Implications of Mn Deficiency for Mn Binding in Various PSII Complexes

A marked decrease in the Mn signals was observed along with increasing Mn deficiency in both genotypes (Fig. 4, A and B). Also, the distribution of PSII monomers, dimers, and supercomplexes varied considerably among the Mn treatments (Fig. 4, A and B). By quantifying Mn binding in PSII representing the total amount of fractionated PSII complexes (Fig. 4C), the method provided direct information about biofunctional Mn in contrast to traditional analysis of total leaf Mn concentrations as shown in Figure 4D. This highlights the sensitivity of the method compared with traditional approaches. It also shows the possibility to study the dynamics of PSII complexes and quantify the biofunctional pool of photosynthetic metals in general.

The decreasing levels of PSII complexes as a consequence of Mn deficiency were supported by BN-PAGE gels (Fig. 5), showing that PSII-LHCII supercomplexes were the primary target of Mn deficiency. The amount of PSII-LHCII supercomplexes decreased drastically in response to Mn deficiency for both genotypes, and at the end of the experimental period, the level of PSII-LHCII supercomplexes was decreased to negligible amounts in plants grown under severe Mn deficiency (Figs. 4, A and B and 5, lane 4).

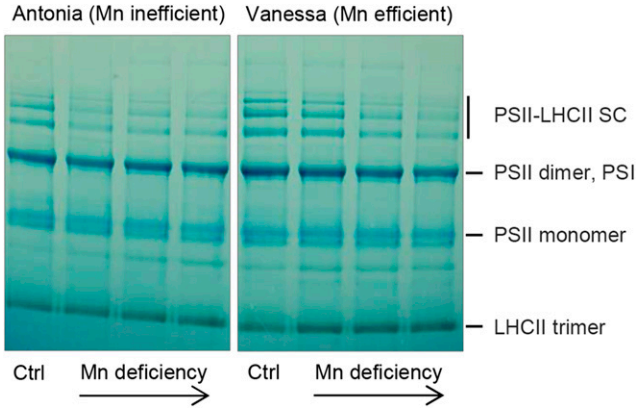

Figure 5. BN-PAGE gels showing the separation of β-DM-solubilized thylakoid membrane complexes from plants grown with sufficient Mn supply (control [Ctrl]) or under mild, moderate, or severe Mn deficiency (lanes 1–4, respectively). Left, The Mn-inefficient genotype cv Antonia. Right, The Mn-efficient genotype cv Vanessa; 15 μg of protein was loaded on each lane. SC, Supercomplex.

Despite the large decrease in Mn binding in PSII under Mn deficiency, the deficiency seemed latent, with no visual symptoms, except for slightly chlorotic leaves of the plants exposed to severe Mn deficiency. Plants of both genotypes displayed strongly reduced quantum yield efficiencies of PSII (variable fluorescence [F_v] to maximal fluorescence [F_m] ratio) with increasing Mn deficiency (Supplemental Table S2) ranging between 0.55 and 0.58 for plants exposed to severe Mn deficiency. An F_v to F_m ratio of 0.55 has previously been found to constitute the threshold limit for development of visible leaf symptoms in hydroponically grown barley plants (Husted et al., 2009). The minimal fluorescence increased significantly when plants were exposed to increasing level of Mn deficiency, indicating photoinhibition (Supplemental Table S2).

Genotypic Differences with Respect to Mn Binding in PSII Complexes

The Mn-efficient genotype cv Vanessa contained significantly more Mn in PSII under control and mild Mn deficiency conditions than the inefficient genotype cv Antonia (Fig. 4C). However, under moderate and severe Mn deficiency, genotypic differences with respect to Mn binding in PSII were no longer observed (Fig. 4C).

When the two contrasting genotypes were grown under control and mild Mn deficiency, it was clear that fewer PSII-LHCII supercomplexes were formed in the Mn-inefficient genotype cv Antonia compared with cv Vanessa under those conditions (Fig. 5, lanes 1 and 2). This observation was in agreement with the decrease in the relative Mn intensity of the fraction representing PSII-LHCII supercomplexes (Fig. 4A, supercomplexes versus Fig. 4B, supercomplexes). At moderate and severe Mn deficiency, the amounts of PSII super- and subcomplexes were reduced to similar levels in both genotypes (Fig. 5, lanes 3 and 4).

The fact that more Mn was bound in PSII under control and mild Mn deficiency conditions in one genotype (cv Vanessa) compared with another genotype (cv Antonia) raises the question if cv Vanessa has more PSII compared with cv Antonia. Analytically, this question was investigated by determining the relative amount of incorporated Mn in PSII per unit of S (proxy for protein) across the different Mn-containing fractions (Fig. 6).

The efficient genotype cv Vanessa clearly incorporated more Mn per unit of protein S under control and mild Mn deficiency conditions (Fig. 6, A and B), implying higher amounts of functional PSII in cv Vanessa compared with cv Antonia. This observation is in close agreement with the higher Mn binding shown in Figure 4B. The Chl *a* to Chl *b* ratio is an indicator of the relative ratio of PSI to PSII but is also dependent on the core to LHCII ratio (Chl *b* is generally more abundant in LHCII), thereby also being an indicator of the antenna size. The Chl *a* to Chl *b* ratio was not significantly different between the genotypes in the different treatments (Supplemental Table S2), showing that the same amount of PSI relative to PSII was

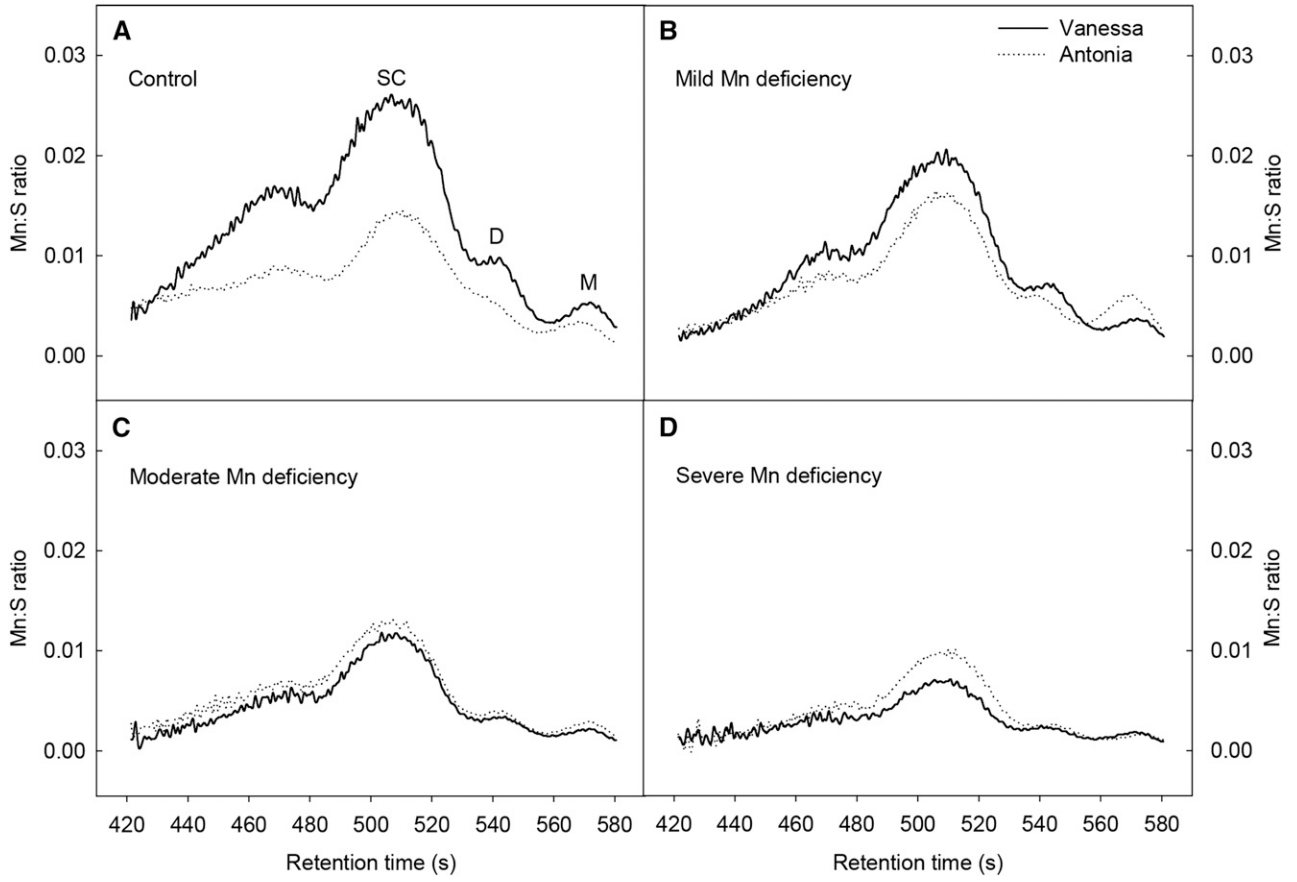

Figure 6. SEC-ICP-QQQ-MS chromatograms showing the Mn and S stoichiometric ratios of thylakoids isolated from cv Antonia and cv Vanessa plants grown as control (A) or under mild (B), moderate (C), or severe (D) Mn deficiency conditions. Fractionated PSII complexes were indexed as follows: PSII-LHCII supercomplex (SC), dimer (D), and monomer (M).

loaded onto the column for both genotypes in each treatment. When evaluating total Chl content (Chl *a* + *b*; Supplemental Table S2), data indicated that more Chl per protein was loaded for cv Vanessa compared with cv Antonia under control and mild Mn deficiency, which could explain the higher amount of PSII-LHCII supercomplexes in cv Vanessa compared with cv Antonia. However, for cv Antonia, the Mn to S stoichiometry data indicated more complexes without a functional Mn cluster attached, which could be attributable to differences in repair and/or assembly processes of PSII compared with cv Vanessa. Other possibilities could be a decreased transport of Mn from storage pools (e.g. vacuoles) or insufficient transfer of Mn from the chloroplast stroma to the luminal side of PSII in the thylakoids.

Genotypic Differences with Respect to Mn Use Efficiency

Mn efficiency has so far only been related to root acquisition of Mn (e.g. mediated by transport proteins; Pedas et al., 2005, 2008; Ihnatowicz et al., 2014) or mobilization of soil Mn through exudation of phytases and organic acid anions (Rengel and Marschner, 2005; George et al., 2014). We observed a striking difference in Mn binding in PSII between the two genotypes for plants grown under control conditions or mild Mn deficiency (Fig. 4C). Total leaf Mn concentrations did not differ significantly between the genotypes irrespective of the degree of Mn deficiency (Fig. 4D); however, cv Antonia had a higher leaf Mn concentration than cv Vanessa in the control treatment. Until now, Mn efficiency has not been associated with differences in internal allocations and functional requirements of Mn (Graham et al., 1985; Marcar and Graham, 1987). The fact that cv Vanessa bound more Mn in PSII, despite having a lower or similar leaf Mn concentration under control and mild Mn deficiency, respectively, showed a more efficient use or more efficient binding of Mn in PSII in the Mn-efficient genotype cv Vanessa. Hence, a better internal use of Mn may contribute to Mn efficiency. Furthermore, it can be concluded that total leaf Mn concentration is an inadequate measure of bioavailable Mn in planta (Fig. 4C versus Fig. 4D), although leaf Mn concentrations responded significantly to limited Mn availability for both genotypes (Fig. 4D). Any attempt to further investigate Mn transport routes and PSII assembly pathways must take into account the variability imposed

by changes in the bioavailability of Mn (Salomon and Keren, 2011).

CONCLUSION

In this work, we have established and verified a novel method that allows sensitive and simultaneous analysis of biometals in size-fractionated photosynthetic complexes from barley thylakoids. The method is able to unravel the dynamic changes in abundance of various PSII supercomplexes and state of multimerization as exemplified by the relative distribution of PSII dimers and monomers.

The analytical strength of the method was shown using a biological case where barley genotypes with contrasting Mn efficiency were exposed to increasing levels of Mn deficiency. The analysis of these plants showed that the method opens up for new experiments on the internal use of Mn and other biometals in various PSII and PSI complexes as well as their relative dynamics according to changes in environmental conditions and genetic background. Moreover, the method constitutes a useful addition to the studies of assembly and function of thylakoid pigment-protein complexes because these are highly dependent on metal cofactor incorporation.

MATERIALS AND METHODS

Plant Material and Isolation of Thylakoid Membranes

Barley (*Hordeum vulgare* 'Antonia' and 'Vanessa') plants were germinated in vermiculite for 6 d (5 d at 28°C/25°C and 1 d at 18°C/15°C day-night temperature cycles). The seedlings were transferred to 4-L cultivation units and grown hydroponically in a nutrient solution that was aerated continuously and renewed weakly (Schmidt et al., 2013). Mn was supplied separately on a daily basis, and Mn deficiency was gradually induced (Mn deficiency experiment). The plants were grown for 31 d (plants used for method development) or 39 d (Mn deficiency experiment) in a greenhouse under the following conditions: 16-h daylength and 18°C/15°C day-night temperature cycle. Before harvest, the plants were dark adapted (approximately 7 h) to reduce the starch content in the leaves. The youngest fully emerged leaves from each cultivation unit were sampled and pooled to obtain a sufficient amount of leaf material. Leaf samples were frozen immediately in liquid nitrogen and stored at −80°C until further preparation.

Wild-type and *viridis zb63* barley plants were germinated and grown in vermiculite in a greenhouse for 9 d at a 16-h daylength and 18°C/15°C day-night temperature cycle. Homozygous mutant plants were easily distinguished from the wild type by their paler green color. Before harvest, plants were dark adapted (approximately 18 h).

Thylakoid membranes were isolated by disrupting leaf samples in a razor-blade blender in the presence of ice-cold homogenization buffer (0.2 M Suc, 10 mM NaCl, 5 mM $MgCl_2$, 20 mM Tricine, pH 7.9, 10 mM ascorbate, and 10 mM NaF) under dim green light. The suspension was filtered through two layers of Miracloth and subsequently centrifuged at 6,000*g* for 10 min at 4°C. The pellet was resuspended in Tricine buffer (5 mM Tricine, pH 7.9, and 10 mM NaF) followed by 10 min of centrifugation at 11,200*g* at 4°C. The resulting thylakoid pellet was suspended in storage buffer (0.2 M Suc, 10 mM NaCl, 5 mM $MgCl_2$, 20 mM Tricine, 10 mM NaF, and 20% [v/v] glycerol) and kept at −80°C until further analysis.

Chl *a* Fluorescence Measurements

Chl *a* fluorescence was recorded with a Plant Efficiency Analyzer (Hansatech) three times per week. The measurements were made on the youngest fully emerged leaves for each plant, and the leaves were dark adapted for 25 min before analysis to ensure that all reaction centers of PSII are in an open state. PSII photochemical efficiency was calculated as the ratio of F_v to F_m.

Thylakoid Solubilization

Thylakoids were solubilized according to the work by Järvi et al. (2011) with a few modifications. After thawing the thylakoids in darkness on ice, the samples were centrifuged at 7,000*g* at 4°C for 2 min and resuspended into ice-cold buffer A (25 mM Bis-Tris-HCl, pH 7, 20% [v/v] glycerol, and 0.25 mg mL^{-1} of Pefabloc) or 25 mM Bis-Tris-HCl, pH 7, 12.5% (v/v) glycerol, 2 M betaine, and 0.25 mg mL^{-1} of Pefabloc to a protein concentration of 2 mg mL^{-1}. An equal volume of detergent solution prepared in buffer A was added to a final concentration of 1% (w/v) α-DM (Affymetrix) or β-DM (Sigma-Aldrich). Thylakoid membranes were solubilized in darkness for 10 min on ice, and insoluble material was removed by centrifugation at 18,000*g* at 4°C for 15 min.

SEC-ICP-QQQ-MS Measurements

The suitability of various SEC columns, including Superdex 75 and 200 HR10/300 GL (dextran-based low-pressure glass columns; Amersham Biosciences) together with BioBasic SEC 300 and SEC 1000 (silica-based high-pressure steel columns; Thermo Scientific), were tested to optimize resolution, recovery of metalloprotein complexes, and the analytical run time. The BioBasic SEC 1000 Column, including a guard column, was selected because of its superior resolution of larger-sized protein complexes (20–4,000 kD *molecular mass* range). The column was size calibrated with standard proteins by UV detection at 280 nm using Thyroglobulin (669 kD), Ferritin (440 kD), Catalase (232 kD), Cu-Zn superoxide dismutase (32.5 kD), and Chymotrypsinogen A (25 kD). The retention times were linearly related to the log of calibration standard *molecular mass* values ($R^2 = 0.96$).

Solubilized thylakoid proteins were passed through a 0.2-μm membrane filter (Sartorius Stedim Biotech) and applied (50 μg when analyzed in oxygen mode or 250 μg for Ca measurements in hydrogen mode) to the SEC column using an inert HPLC system (Ultimate 3000; Dionex; Thermo Scientific). The column temperature was kept at 6°C during analysis. Elution was performed with ice-cold mobile phases: 50 mM AmAc (BioXtra; Sigma-Aldrich), pH 7; 25 mM Tricine (BioXtra; Sigma-Aldrich)-NaOH, pH 7; or 25 mM Bis-Tris (BioXtra; Sigma-Aldrich)-trifluoroacetic acid, pH 7 (occasionally with the addition of 0.5 M betaine) and 0.03% (w/v) α-DM or β-DM as indicated. Proteins were eluted from the column at a flow rate of 1 mL min^{-1}, and they were detected using UV-Vis spectrophotometry at 280, 400, and 663 nm. The outlet of the UV-Vis detector was coupled to an ICP-QQQ-MS (Agilent 8800 ICP-QQQ-MS) for online analysis of metal binding in the size-fractionated thylakoid proteins. The delay time between the UV-Vis and ICP-QQQ-MS detector was far less than 1 s and thereby, without significance. The ICP-QQQ-MS was operated in MS/MS scan mode with either oxygen or hydrogen as the reaction gas, which allowed for ultrasensitive and simultaneous detection of all elements of interest. In MS/MS mode, the first quadrupole strictly controls the atomic species that enter the octopole reaction cell. After reaction with the chosen cell gas, the target analytes or product ions are detected by the last quadrupole, essentially being free from isobaric and polyatomic interferences. The plasma conditions and ion lenses were tuned on a daily basis for robust plasma conditions and maximum sensitivity.

Oxygen Mode

When oxygen is introduced (100% oxygen added at approximately 0.3 mL min^{-1}) into the reaction cell, the resulting mass shift that occurs for some elements produces oxide product ions, which are detected by the last quadrupole. This approach is highly favorable for heavily interfered elements, resulting in greatly improved sensitivity and detection limits. Among the target elements, S and Fe were successfully analyzed as oxide product ions ($^{48}SO^+$ and $^{72}FeO^+$), whereas Mg and Mn were analyzed as the parent ions $^{24}Mg^+$ and $^{55}Mn^+$, with a negligible sensitivity penalty. The integration time was 0.1 s per element.

The external calibration for quantification of the Mn and S stoichiometric ratios in photosynthetic complexes was determined using flow injection analysis. Calibrants of Mn (element standard) and S (Cys) were mixed at Mn:S ranging from 1:20 to 1:200 in mobile-phase buffer (25 mM Bis-Tris-TFA, pH 7, 0.03% [w/v] α-DM, and 1 mM EDTA). The calibrants (50 μL) were injected to the ICP-QQQ-MS through the HPLC system at a flow rate of 1 mL min^{-1} in mobile-phase buffer without EDTA.

Hydrogen Mode

To improve the sensitivity for $^{40}Ca^+$, hydrogen was used (7 mL min^{-1}) as the cell reaction gas. Reactions with hydrogen reduce the background from Ar^+ generated in the plasma at a mass-to-charge ratio of 40 by charge transfer. This reaction chemistry is optimized to specifically direct it toward Ar, whereas Ca, Fe, and Mn do not react with hydrogen under the conditions given, which is why there is no loss in analyte signal. The target elements were analyzed as the parent ions $^{40}Ca^+$, $^{56}Fe^+$, and $^{55}Mn^+$. The integration time was 0.1 s for Mn and Fe and 0.3 s for Ca.

The external calibration for calculation of the molar Mn to Ca ratio in the largest Mn-containing fraction was performed using flow injection analysis. Calibrants of Mn and Ca (single-element standards) were mixed at a 1:1 ratio ranging from 0.75 to 100 μg L^{-1} concentrations in 3.5% (v/v) HNO_3. The calibrants (250 μL) were injected to the ICP-QQQ-MS through the HPLC system at a flow rate of 1 mL min^{-1}, using 3.5% (v/v) HNO_3 as the mobile phase.

Total Mn Concentration in Leaves

Mn concentration in leaves was determined using ICP-optical emission spectroscopy (Optima 5300 DV; PerkinElmer). The youngest fully emerged leaves were homogenized into a fine powder in liquid nitrogen and freeze dried, and a representative sample (approximately 100 mg) was digested using a pressurized microwave digestion system (UltraWAVE; Milestone Srl; Hansen et al., 2009, 2013). The accuracy and precision of the ICP-optical emission spectroscopy measurements were estimated by the analysis of certified reference material (apple [*Malus domestica*] leaf Nist 1515; National Institute of Standards and Technology).

Biochemical Characterization of Collected SEC Fractions

For immunoblot analysis, protein fractions collected from SEC were separated by SDS-PAGE and transferred to an immunoblot polyvinylidene difluoride membrane (Bio-Rad) using the Bio-Rad Criterion Gel System and the Bio-Rad Criterion Blotter. Proteins were immunodetected using a horseradish peroxidase-conjugated secondary antibody and a chemiluminescent detection system (BioSpectrum Imaging System [UVP]) combined with SuperSignal West Dura (Pierce; Thermo Scientific) according to the instructions of the manufacturer. All antibodies were purchased from Agrisera. For BN-PAGE, either 15 μg of solubilized thylakoid protein or an equal volume of each fraction collected from SEC (concentrated using 10-kD cutoff centrifugal filters; Amicon Ultra-4; Millipore) was mixed with a 4× sample buffer (NativePage Novex) and loaded onto a linear gradient gel (NativePAGE Novex; 3%–12% or 4%–16% Bis-Tris protein gels). Anode buffer (50 mM Tricine and 15 mM Bis-Tris-HCl, pH 7)] and cathode buffer (50 mM Tricine, 15 mM Bis-Tris-HCl, pH 7, and 0.02% [w/v] Coomassie Blue G250) were used, and electrophoresis was carried out at 150 V constant for approximately 4 h. For subsequent immunodetection, the BN-PAGE gels were briefly (15 min) put in transfer buffer (25 mM Tris, 192 mM Gly, and 10% [v/v] methanol) including 0.1% (w/v) SDS and then transferred to a polyvinylidene difluoride membrane by electroblotting at 50 V for 45 min. The membranes were destained in 20% (v/v) methanol and 7% (v/v) acetic acid for 2 h, blocked using 5% (w/v) skimmed milk, and incubated with primary antibodies overnight. Proteins were immunodetected as described above.

Oxygen Evolution Rate

Oxygen evolution was measured at 25°C using a Clark-type electrode (Hansatech) under saturated light intensities. Mn-containing fractions were heart cut and concentrated using 10-kD cutoff centrifugal filters (Amicon Ultra-4; Millipore). The samples (10 μg of Chl mL^{-1}) were suspended in 2 mL of O_2 buffer (25 mM MES, pH 6.5, 2 M betaine, 10 mM $NaHCO_3$, 10 mM NaCl, and 25 mM $CaCl_2$) in the presence of 1 mM potassium ferricyanide and 200 μM 2,6-dichlorobenzoquinone.

Analysis of Pigment Composition

Pigments were extracted from thylakoids (50 μg of protein) in 350 μL of acetone:water:25% (v/v) NH_4OH (80:19:1) followed by two centrifugation steps at 20,000*g* for 15 min at 4°C. All samples were carefully flushed with N_2. Pigments were separated on a Zorbax Extend-C18 Column (4.6 × 150 mm, 3.5 μm; Agilent) using a Dionex HPLC System. The mobile phase consisted of two solvents, A (acetonitrile:methanol:water [84:9:7]) and B (methanol:ethylacetate [68:32]), both of which contained 0.1% (v/v) triethylamine. The pigments were eluted starting with a linear gradient from 100% solvent A to 100% solvent B in 10 min followed by isocratic elution with 100% solvent B for 5 min and a linear gradient of 100% solvent B to 100% solvent A in 1 min. The column was regenerated with 100% solvent A for 20 min before injection of the next sample. The injection volume was 40 μL, and the flow rate was 1 mL min^{-1}. The eluate was monitored using photodiode array detection in the range 290 to 595 nm. Peaks were quantified by integration at 445 nm using Chromeleon software (Chromeleon version 6; Dionex).

Proteomic MS Analysis

Mn_1 and Fe_1 fractions were heart cut, concentrated on 100-kD cutoff centrifugal filters (Amicon Ultra-4; Millipore), and stored at −80°C. Upon enzymatic digestion, the samples were thawed on ice in darkness. Then, disulfide bridges were reduced and alkylated by adding dithiothreitol (Sigma-Aldrich) and iodoacetamide (Sigma-Aldrich), respectively. Enzymatic digestion of the proteins was performed by incubation with trypsin (sequence grade; Promega) overnight. Purification and desalting of the samples were performed using Stage Tip, C18 Solid-Phase Extraction Discs (3M Empore). Finally, the samples were dried by rotational vacuum concentration (Christ Alpha RVC; Martin Christ GmbH), and the peptides were resolved in formic acid. The peptides were separated on an EASY-Spray Column (15-cm × 75-μm i.d., 3-μm particles, 100-Å pore size; PepMap C18; Thermo Scientific) using a 60-min gradient prepared from solvent A (0.1% [v/v] formic acid) and solvent B (80% [v/v] acetonitrile in 0.1% [v/v] formic acid) at a flow rate of 100 nL min^{-1} on a NanoLC System (EASY-nLC II; Thermo Scientific) and analyzed by an Orbitrap Q Exactive (Thermo Scientific). The gradient was ramped from 5% to 60% solvent B in 54 min and then increased to 95% for 6 min. The Q Exactive was operated in data-dependent mode with 10 MS/MS spectra for every full scan. The obtained mass spectral data were processed and searched using Proteome Discoverer (version 1.4.0.288) in the barley National Center for Biotechnology Information Protein Database for identification of peptides and proteins. The following search parameters were applied: maximum one missed cleavage site, allowed modification: carbamidomethylated Cys (static) and oxidation of Met (dynamic), and peptide mass tolerance in MS and MS/MS: 10 μL L^{-1} and 0.6 D, respectively. The threshold for positive identification of proteins by MS/MS analysis was set to a minimum of three unique peptides, with at least one peptide having a significant ion score.

Data Analysis

Statistical analysis was performed using SAS (version 9.4; SAS Institute) for variance analysis and Student's *t* test for comparison of means of leaf Mn concentrations, pigment, and fluorescence data. Three independent replicates were included in the analyses.

Peak Fitting and Optimization Procedure for Mn to Ca Ratio Determination

The molar Mn to Ca ratio was calculated based on peak areas in four independent thylakoid samples. The area of the first eluting Mn and Ca peak was determined by fitting the chromatographic data for Mn and Ca ion intensities. It was assumed that each peak can be fitted using the commonly used EMG profile described by Equation 1 (Di Marco and Bombi, 2001):

$$y = \frac{hw}{s}\sqrt{\frac{\pi}{2}}\exp\left(\frac{w^2}{2s^2}-\frac{x-z}{s}\right)\left\{1-\mathrm{erf}\left[\frac{1}{\sqrt{2}}\left(\frac{w}{s}-\frac{x-z}{w}\right)\right]\right\} \quad (1)$$

where erf is the error function given by

$$\mathrm{erf}(x) = \frac{2}{\sqrt{\pi}}\int_0^x e^{-t^2}dt$$

Here, y is the predicted intensity of the chromatographic peak, and x is the retention time. The four parameters that are optimized for each profile are related to peak height (h), the retention time of the peak (z), the symmetry of the peak (s), and the width of the peak (w). For the Mn signal, the sum of three separate EMG profiles was used to fit the three visible peaks in the chromatographic signal. For the Ca signal, the sum of two separate EMG profiles

was used to fit the two visible Ca peaks in the chromatogram. The fitted curve was optimized using the constrained Simulated Annealing function simulannealbnd in Matlab R2014b (Mathworks Inc.). For each of four samples, this optimization procedure was run 15 times for each element, and the best fit for each element was chosen as the one giving the lowest root mean squared error between the fit and the measured signal. The molar Mn to Ca ratio for the first Mn and Ca peak was calculated based on the area of the corresponding fitted peaks.

Supplemental Data

The following supplemental materials are available.

Supplemental Figure S1. Chromatographic signals for Mn and Ca.

Supplemental Figure S2. Molar Mn to Ca ratio signals.

Supplemental Figure S3. Peak fittings of Mn and Ca signals.

Supplemental Figure S4. Spectroscopic characteristics.

Supplemental Figure S5. Wild-type and *viridis zb63* elution profiles.

Supplemental Figure S6. Chromatographic signals for Mn, Fe, and Ca measured in H_2-mode.

Supplemental Table S1. MS identification of heart-cut fractions.

Supplemental Table S2. Photosynthetic parameters.

ACKNOWLEDGMENTS

We thank Lena Byrgesen and Thomas H. Hansen for assistance with the element analysis and Birgit Andersen for assistance with the MS analysis and protein identification.

Received April 15, 2015; accepted June 15, 2015; published June 17, 2015.

LITERATURE CITED

Barera S, Pagliano C, Pape T, Saracco G, Barber J (2012) Characterization of PSII-LHCII supercomplexes isolated from pea thylakoid membrane by one-step treatment with α- and β-dodecyl-D-maltoside. Philos Trans R Soc Lond B Biol Sci **367:** 3389–3399

Boekema EJ, Hankamer B, Bald D, Kruip J, Nield J, Boonstra AF, Barber J, Rögner M (1995) Supramolecular structure of the photosystem II complex from green plants and cyanobacteria. Proc Natl Acad Sci USA **92:** 175–179

Boekema EJ, Nield J, Hankamer B, Barber J (1998) Localization of the 23-kDa subunit of the oxygen-evolving complex of photosystem II by electron microscopy. Eur J Biochem **252:** 268–276

Bricker TM, Roose JL, Fagerlund RD, Frankel LK, Eaton-Rye JJ (2012) The extrinsic proteins of Photosystem II. Biochim Biophys Acta **1817:** 121–142

Caffarri S, Kouril R, Kereïche S, Boekema EJ, Croce R (2009) Functional architecture of higher plant photosystem II supercomplexes. EMBO J **28:** 3052–3063

Dekker JP, Germano M, van Roon H, Boekema EJ (2002) Photosystem II solubilizes as a monomer by mild detergent treatment of unstacked thylakoid membranes. Photosynth Res **72:** 203–210

Di Marco VB, Bombi GG (2001) Mathematical functions for the representation of chromatographic peaks. J Chromatogr A **931:** 1–30

Eshaghi S, Andersson B, Barber J (1999) Isolation of a highly active PSII-LHCII supercomplex from thylakoid membranes by a direct method. FEBS Lett **446:** 23–26

George TS, French AS, Brown LK, Karley AJ, White PJ, Ramsay L, Daniell TJ (2014) Genotypic variation in the ability of landraces and commercial cereal varieties to avoid manganese deficiency in soils with limited manganese availability: is there a role for root-exuded phytases? Physiol Plant **151:** 243–256

Graham RD, Davies WJ, Ascher JS (1985) The critical concentration of manganese in field-grown wheat. Aust J Agric Res **36:** 145–155

Grotjohann I, Fromme P (2005) Structure of cyanobacterial photosystem I. Photosynth Res **85:** 51–72

Hansen TH, de Bang TC, Laursen KH, Pedas P, Husted S, Schjoerring JK (2013) Multielement plant tissue analysis using ICP spectrometry. Methods Mol Biol **953:** 121–141

Hansen TH, Laursen KH, Persson DP, Pedas P, Husted S, Schjoerring JK (2009) Micro-scaled high-throughput digestion of plant tissue samples for multi-elemental analysis. Plant Methods **5:** 12

Heinemeyer J, Eubel H, Wehmhöner D, Jänsch L, Braun HP (2004) Proteomic approach to characterize the supramolecular organization of photosystems in higher plants. Phytochemistry **65:** 1683–1692

Husted S, Laursen KH, Hebbern CA, Schmidt SB, Pedas P, Haldrup A, Jensen PE (2009) Manganese deficiency leads to genotype-specific changes in fluorescence induction kinetics and state transitions. Plant Physiol **150:** 825–833

Husted S, Persson DP, Laursen KH, Hansen TH, Pedas P, Schiller M, Hegelund JN, Schjoerring JK (2011) Review: the role of atomic spectrometry in plant science. J Anal At Spectrom **26:** 52–79

Ifuku K, Ido K, Sato F (2011) Molecular functions of PsbP and PsbQ proteins in the photosystem II supercomplex. J Photochem Photobiol B **104:** 158–164

Ihnatowicz A, Siwinska J, Meharg AA, Carey M, Koornneef M, Reymond M (2014) Conserved histidine of metal transporter AtNRAMP1 is crucial for optimal plant growth under manganese deficiency at chilling temperatures. New Phytol **202:** 1173–1183

Järvi S, Gollan PJ, Aro EM (2013) Understanding the roles of the thylakoid lumen in photosynthesis regulation. Front Plant Sci **4:** 434

Järvi S, Suorsa M, Aro EM (2015) Photosystem II repair in plant chloroplasts:regulation, assisting proteins and shared components with photosystem II biogenesis. Biochim Biophys Acta **1847:** 900–909

Järvi S, Suorsa M, Paakkarinen V, Aro EM (2011) Optimized native gel systems for separation of thylakoid protein complexes: novel super- and mega-complexes. Biochem J **439:** 207–214

Jordan P, Fromme P, Witt HT, Klukas O, Saenger W, Krauss N (2001) Three-dimensional structure of cyanobacterial photosystem I at 2.5 A resolution. Nature **411:** 909–917

Kouřil R, Dekker JP, Boekema EJ (2012) Supramolecular organization of photosystem II in green plants. Biochim Biophys Acta **1817:** 2–12

Liu H, Zhang H, Weisz DA, Vidavsky I, Gross ML, Pakrasi HB (2014) MS-based cross-linking analysis reveals the location of the PsbQ protein in cyanobacterial photosystem II. Proc Natl Acad Sci USA **111:** 4638–4643

Marcar NE, Graham RD (1987) Genotypic variation for manganese efficiency in wheat. J Plant Nutr **10:** 2049–2055

Marr KM, McFeeters RL, Lyon MK (1996) Isolation and structural analysis of two-dimensional crystals of photosystem II from Hordeum vulgare viridis zb63. J Struct Biol **117:** 86–98

Merchant S (2006) Trace metal utilization in chloroplasts. *In* R Wise, JK Hoober, eds, The Structure and Function of Plastids, Vol 23. Springer, Dordrecht, The Netherlands, pp 199–218

Møller IM, Jensen PE, Hansson A (2007) Oxidative modifications to cellular components in plants. Annu Rev Plant Biol **58:** 459–481

Morosinotto T, Bassi R, Frigerio S, Finazzi G, Morris E, Barber J (2006) Biochemical and structural analyses of a higher plant photosystem II supercomplex of a photosystem I-less mutant of barley: consequences of a chronic over-reduction of the plastoquinone pool. FEBS J **273:** 4616–4630

Nelson N, Yocum CF (2006) Structure and function of photosystems I and II. Annu Rev Plant Biol **57:** 521–565

Nielsen VS, Scheller HV, Møller BL (1996) The photosystem I mutant viridis-zb(63) of barley (Hordeum vulgare) contains low amounts of active but unstable photosystem I. Physiol Plant **98:** 637–644

Nouet C, Motte P, Hanikenne M (2011) Chloroplastic and mitochondrial metal homeostasis. Trends Plant Sci **16:** 395–404

Ono TA, Noguchi T, Inoue Y, Kusunoki M, Matsushita T, Oyanagi H (1992) X-ray detection of the period-four cycling of the manganese cluster in photosynthetic water oxidizing enzyme. Science **258:** 1335–1337

Pagliano C, Barera S, Chimirri F, Saracco G, Barber J (2012) Comparison of the α and β isomeric forms of the detergent n-dodecyl-D-maltoside for solubilizing photosynthetic complexes from pea thylakoid membranes. Biochim Biophys Acta **1817:** 1506–1515

Pagliano C, Chimirri F, Saracco G, Marsano F, Barber J (2011) One-step isolation and biochemical characterization of a highly active plant PSII monomeric core. Photosynth Res **108:** 33–46

Pagliano C, Nield J, Marsano F, Pape T, Barera S, Saracco G, Barber J (2014) Proteomic characterization and three-dimensional electron microscopy study of PSII-LHCII supercomplexes from higher plants. Biochim Biophys Acta **1837:** 1454–1462

Pakrasi H, Ogawa T, Bhattacharrya-Pakrasi M (2001) Transport of metals: a key process in oxygenic photosynthesis. *In* EM Aro, B Andersson, eds, Regulation of Photosynthesis, Vol 11. Springer, Dordrecht, The Netherlands, pp 253–264

Papageorgiou GC, Fujimura Y, Murata N (1991) Protection of the oxygen-evolving photosystem-II complex by glycine betaine. Biochim Biophys Acta **1057:** 361–366

Papageorgiou GC, Murata N (1995) The unusually strong stabilizing effects of glycine betaine on the structure and function of the oxygen-evolving Photosystem II complex. Photosynth Res **44:** 243–252

Pedas P, Hebbern CA, Schjoerring JK, Holm PE, Husted S (2005) Differential capacity for high-affinity manganese uptake contributes to differences between barley genotypes in tolerance to low manganese availability. Plant Physiol **139:** 1411–1420

Pedas P, Ytting CK, Fuglsang AT, Jahn TP, Schjoerring JK, Husted S (2008) Manganese efficiency in barley: identification and characterization of the metal ion transporter HvIRT1. Plant Physiol **148:** 455–466

Persson DP, Hansen TH, Laursen KH, Schjoerring JK, Husted S (2009) Simultaneous iron, zinc, sulfur and phosphorus speciation analysis of barley grain tissues using SEC-ICP-MS and IP-ICP-MS. Metallomics **1:** 418–426

Raven J, Evans MW, Korb R (1999) The role of trace metals in photosynthetic electron transport in O2-evolving organisms. Photosynth Res **60:** 111–149

Rengel Z, Marschner P (2005) Nutrient availability and management in the rhizosphere: exploiting genotypic differences. New Phytol **168:** 305–312

Roose JL, Wegener KM, Pakrasi HB (2007) The extrinsic proteins of Photosystem II. Photosynth Res **92:** 369–387

Salomon E, Keren N (2011) Manganese limitation induces changes in the activity and in the organization of photosynthetic complexes in the cyanobacterium *Synechocystis* sp. strain PCC 6803. Plant Physiol **155:** 571–579

Scheller HV, Jensen PE, Haldrup A, Lunde C, Knoetzel J (2001) Role of subunits in eukaryotic Photosystem I. Biochim Biophys Acta **1507:** 41–60

Schmidt SB, Pedas P, Laursen KH, Schjoerring JK, Husted S (2013) Latent manganese deficiency in barley can be diagnosed and remediated on the basis of chlorophyll *a* fluorescence measurements. Plant Soil **372:** 417–429

Shcolnick S, Keren N (2006) Metal homeostasis in cyanobacteria and chloroplasts: balancing benefits and risks to the photosynthetic apparatus. Plant Physiol **141:** 805–810

Shi LX, Hall M, Funk C, Schröder WP (2012) Photosystem II, a growing complex: updates on newly discovered components and low molecular mass proteins. Biochim Biophys Acta **1817:** 13–25

Tikkanen M, Nurmi M, Kangasjärvi S, Aro EM (2008) Core protein phosphorylation facilitates the repair of photodamaged photosystem II at high light. Biochim Biophys Acta **1777:** 1432–1437

Tokutsu R, Kato N, Bui KH, Ishikawa T, Minagawa J (2012) Revisiting the supramolecular organization of photosystem II in Chlamydomonas reinhardtii. J Biol Chem **287:** 31574–31581

Umena Y, Kawakami K, Shen JR, Kamiya N (2011) Crystal structure of oxygen-evolving photosystem II at a resolution of 1.9 Å. Nature **473:** 55–60

van Roon H, van Breemen JFL, de Weerd FL, Dekker JP, Boekema EJ (2000) Solubilization of green plant thylakoid membranes with n-dodecyl-alpha,D-maltoside. Implications for the structural organization of the Photosystem II, Photosystem I, ATP synthase and cytochrome b6 f complexes. Photosynth Res **64:** 155–166

Yruela I (2013) Transition metals in plant photosynthesis. Metallomics **5:** 1090–1109